J Porous Mater (2010) 17:79–84
DOI 10.1007/s10934-009-9266-7

Template-free fabrication of porous zinc oxide hollow spheres and their enhanced photocatalytic performance

Ming Wang · Xueli Cao · Linjiang Wang · Lide Zhang

Published online: 10 February 2009

Abstract Porous zinc oxide (ZnO) hollow spheres have been fabricated by calcination of a precursor complex in a furnace. The precursor was precipitated in a chemical solution at 80 °C. The field-emission scanning electron microscope and transmission electron microscope reveal the porous and hollow structure of the samples. The spherical hollow precursor is self-assembled in the solution under the coordination effect of citrate ions and the Kirkendall effect working together. The precursors can be converted to pure ZnO crystals by heating in a furnace above 300 °C. The Brunauer–Emmett–Teller (BET) specific surface area of this sample is 95.4 m^2/g. The photocatalytic degradation of methyl blue solution test shows the ZnO hollow spheres have superior photocatalytic activity.

Keywords Nanostructures · Chemical synthesis · Electron microscopy · Photocatalytic activity

M. Wang (✉) · X. Cao · L. Wang
Key Laboratory of New Processing Technology for Nonferrous Metals and Materials, Ministry of Education, Guilin, Guangxi 541004, People's Republic of China
e-mail: wangming@glite.edu.cn

M. Wang · L. Wang
Department of Materials and Chemical Engineering, Guilin University of Technology, Guilin, Guangxi 541004, People's Republic of China

L. Zhang
Key Laboratory of Materials Physics, Institute of Solid State Physics, Chinese Academy of Sciences, Hefei, Anhui 230031, People's Republic of China

1 Introduction

In recent years, hollow spherical materials have attracted tremendous interest due to their advantageous properties including high specific surface area, low density, and good permeation [1–3]. Such merits are of great interest as possible applications in drug delivery, catalysis, sensors, filters, coatings, and so on [4–7]. Generally, templates such as silica spheres [8], polymer spheres [9], liquid and emulsion droplets [10, 11], have been used to synthesize hollow spherical materials. However, the templates remain in the system and need to be removed by further complicated treatments [12]. Therefore, the direct template-free or self-templated synthesis of hollow spheres is urgently needed and continues to be a challenging task.

ZnO, due to its unique properties which include wide direct band gap, large exciton binding energy, piezoelectric and semiconducting properties, has been intensively investigated for its potentially wide range of applications [13]. Different ZnO nanostructures such as belts, tubes, wires, disks, rings, and hierarchical structures have been reported [14–17]. In contrast to the most often studied one-dimensional (1D) ZnO nanomaterials, the reproductive synthesis of hollow spherical structures has received less attention. In the past, only a few groups have reported fabrication of ZnO hollow spheres. Among them, Xie et al. [18] reported hollow spherical ZnO aggregated with small nanoparticles using the hydrothermal method. Li et al. [19] fabricated ZnO hollow spheres by conversion of ZnSe spheres at 600 °C. Huang et al. [20] synthesized ZnO hollow spheres by an autoclave and pyrolysis process.

This paper shows how a porous and hollow structure of ZnO precursor materials has been synthesized utilizing a facile aqueous solution method at low temperature without any template, and which can then be converted to ZnO

crystals by a simple calcination process. Compared with other methods for fabrication of hollow spheres, this method is simple and easy to scale up for production. The photocatalytic degradation test indicates the porous ZnO hollow spheres have good photocatalytic activity due to their high specific surface area, a feature which would be useful in a wide range of applications, such as in drug carriers, chemical reactors, and particularly, catalysis.

2 Experimental section

All of the reagents (analytical grade purity) were purchased from Shanghai Chemical Co. They were used as received without any further purification. The hollow spherical precursor was synthesized as follows: in a typical experiment, 0.66 g zinc acetate, 0.42 g hexamethylenetetramine, and 0.1 g sodium citrate were dissolved in a bottle of 100 mL deionized water. The solution was then kept at 80 °C for 3 h. The resulting precipitation was collected and washed several times with deionized water. The precursor was put in a ceramic boat and was loaded into a furnace. The furnace was heated to 300–500 °C and kept at this temperature for 2 h.

The phase and morphologies of the samples were examined by means of X-ray diffraction (XRD, Philips X'Pert Pro diffractometer with Cu Ka Radiation), field-emission scanning electron microscope (FE-SEM, FEI, Sirion) and transmission electron microscope (TEM JEOL-2010). The composition of the samples was determined by energy dispersive X-ray spectroscopy (EDS, Inca Oxford, attached to the FE-SEM). The thermal decomposition of the precursor was studied using a thermogravimetric analysis (TGA) apparatus with a heating rate of 10 °C/min. The Fourier transform infrared (FT-IR) spectra of the samples were recorded on a Nexus spectrometer with Xe lamp at room temperature. The nitrogen sorption and pore sizes were measured using a Micrometrics ASAP2020 system. The photocatalytic performance was determined by UV–vis absorption spectra (Cary-5E).

3 Result and discussion

3.1 Morphologies and structures

Figure 1 shows XRD patterns of the samples synthesized under optimal conditions (the mole ratio of Zn^{2+}: hexamethylenetetramine: citrate was 10:10:1). No sharp diffraction peak was detected in the as-synthesized precursor sample (line a), indicating the non-crystalline character of the precursor. After annealing at 300 °C for 2 h (line b), several broad diffraction peaks appeared and they can be indexed to wurtzite ZnO (JCPDS No. 36-1451), showing the precursor has been converted to ZnO. With the increase of the annealing temperature to 500 °C (line c), the intensities of ZnO diffraction peaks became stronger. This indicates the improvement of crystalline quality and complete conversion of ZnO.

Figure 2 shows FE-SEM images of the precursor (a, b) and annealed samples (c, d) synthesized under optimal conditions. From the low magnification image of Fig. 2a, it can be observed that a large number of well dispersed spheres with an average diameter of 5 μm were produced. A regular sphere with net-like surface is presented in Fig. 2b and an incompletely formed sphere is displayed in the inset of Fig. 2b, showing the porous and hollow structure of the spheres. Figure 2c and d show the structures and morphologies of the samples annealed at 300 °C and 500 °C, respectively. It can be observed that the surfaces of both the annealed samples have become more coarse. The composition of the sample was tested by EDS. Three elements: zinc, carbon, oxygen were detected in the precursor sample, while only zinc and oxygen were detected in the annealed sample. This shows the precursor is a citrate complex containing the carbon element.

Further morphological observation was carried out by TEM. The samples synthesized under optimal conditions were dispersed in alcohol by ultrasonic agitation for 30 min. Figure 3a shows the TEM image of a single precursor hollow sphere. Obviously, the hollow and porous structures were presented clearly. The inside and outside diameters of the hollow sphere are about 1 and 3 micrometers, respectively. Figure 3b shows the image of a sample annealed at 300 °C for 2 h. The sample annealed at 500 °C was damaged during the ultrasonic agitation

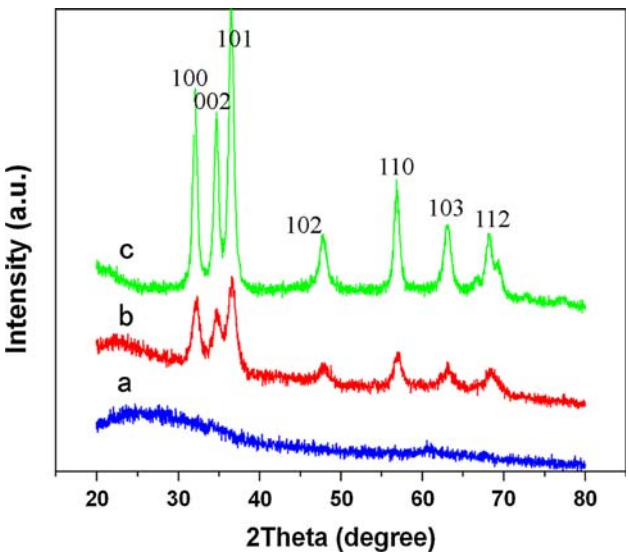

Fig. 1 XRD patterns of the as-synthesized sample (line a), the sample annealed at 300 °C for 2 h (line b), and the sample annealed at 500 °C for 2 h (line c)

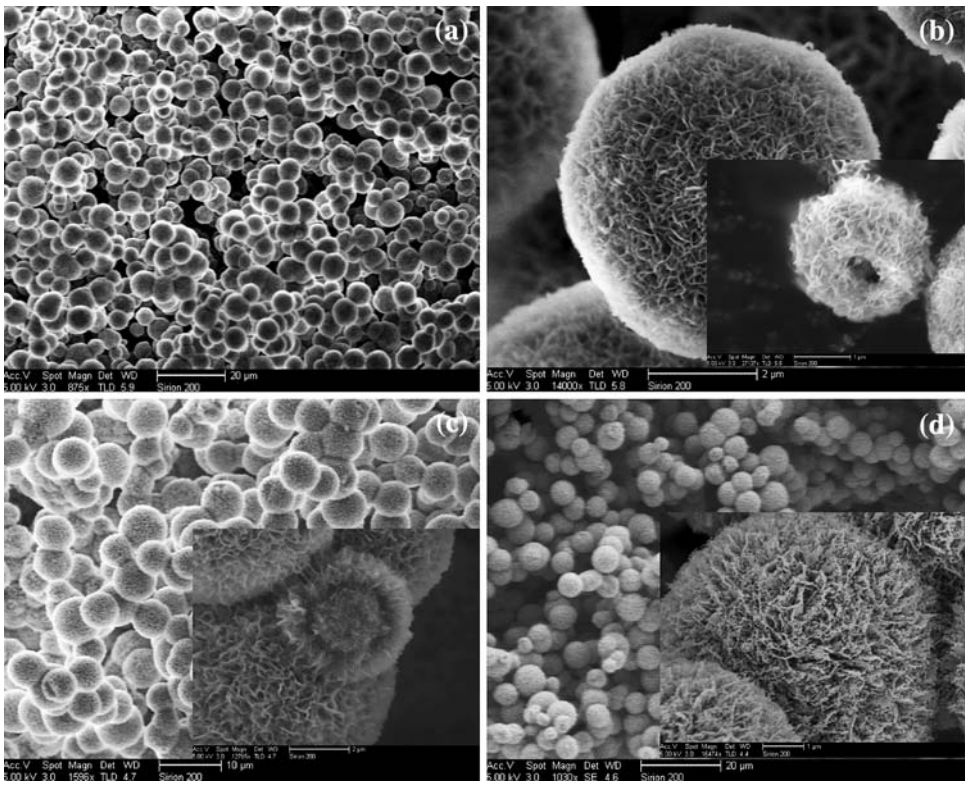

Fig. 2 FE-SEM images of the samples. The structure of the as-synthesized precursor spheres (**a**), the high magnification image of a sphere selected from **a** (inset showing an incompletely formed precursor sphere) (**b**), the structure of the sample annealed at 300 °C (**c**), and the structure of the sample annealed at 500 °C (**d**)

process, yielding the broken fragments of spherical structure shown in Fig. 3c. The selected area electron diffraction of Fig. 3d taken from the small particles shown in Fig. 3c indicates the polycrystalline nature of the ZnO nanocrystals.

3.2 Possible formation mechanism

In general, the fabrication of hollow spheres can be divided into two methods: template and template-free. In the latter method, the formation mechanism is more complicated and little understood. A mechanism analogous to the Kirkendall effect has been widely accepted as that occurring in the formation of hollow spheres in the template-free system [21]. Originally, the Kirkendall effect was referred to as the movement of the interface between a diffusion couple, i.e., copper and zinc in brass, as the result of the different diffusion rates of these two species at an elevated temperature [22]. Later, it was deemed to be the directional material flows resulting from coupled reaction-diffusion phenomena at solid/gas or solid/liquid interfaces, leading to deformation and void formation, which produce pores in the system. This was developed as a method for preparing porous metal oxide materials [23]. In our experiment, the solution contains many species, including gas dissolved in the solution. Thus the phenomena analogous to the Kirkendall effect might appear during the formation of hollow spheres. It was also found that the citrate ion and its mole ratio to Zn^{2+} play a key role in the formation of hollow spheres. Figure 4 shows the SEM image and XRD pattern of the sample obtained without the addition of citrate. The result indicates the product is a crystalline ZnO spindle. In this chemical solution, the hexamethylenetetramine decomposed into formaldehyde and ammonia, which acted as a pH buffer to regulate the pH value of the solution and also provided a small but constant supply of OH^-. The OH^- coordinated with Zn^{2+} to form zinc hydrate, which dehydrated at about 80 °C. The main chemical process can be described as follows: [17]

$$(CH_2)_6N_4 + 6H_2O \rightarrow 6HCHO + 4NH_3 \quad (1)$$

$$NH_3 + H_2O \rightarrow NH_4^+ + OH^- \quad (2)$$

$$2OH^- + Zn^{2+} \rightarrow Zn(OH)_2 \quad (3)$$

$$Zn(OH)_2 \rightarrow ZnO + H_2O \quad (4)$$

When a suitable amount of citrate (the ratio of Zn^{2+}: citrate is 10:1) was added, the carboxyl of citrate was likely to coordinate with Zn^{2+} to form the citrate complex. Thus the hollow spheres were produced by self-assembly of the citrate complex. In reference 18, it was reported that the coordination polymer can react with Zn^{2+} to form hollow spheres. Recently, Wu et al. [24] also found that histidine coordinated with Zn^{2+} to form hollow spheres when its molar ratio was adjusted. Thus in our work, it was thought the working-together of coordination effect and Kirkendall effect are the possible reasons for the formation of hollow spheres.

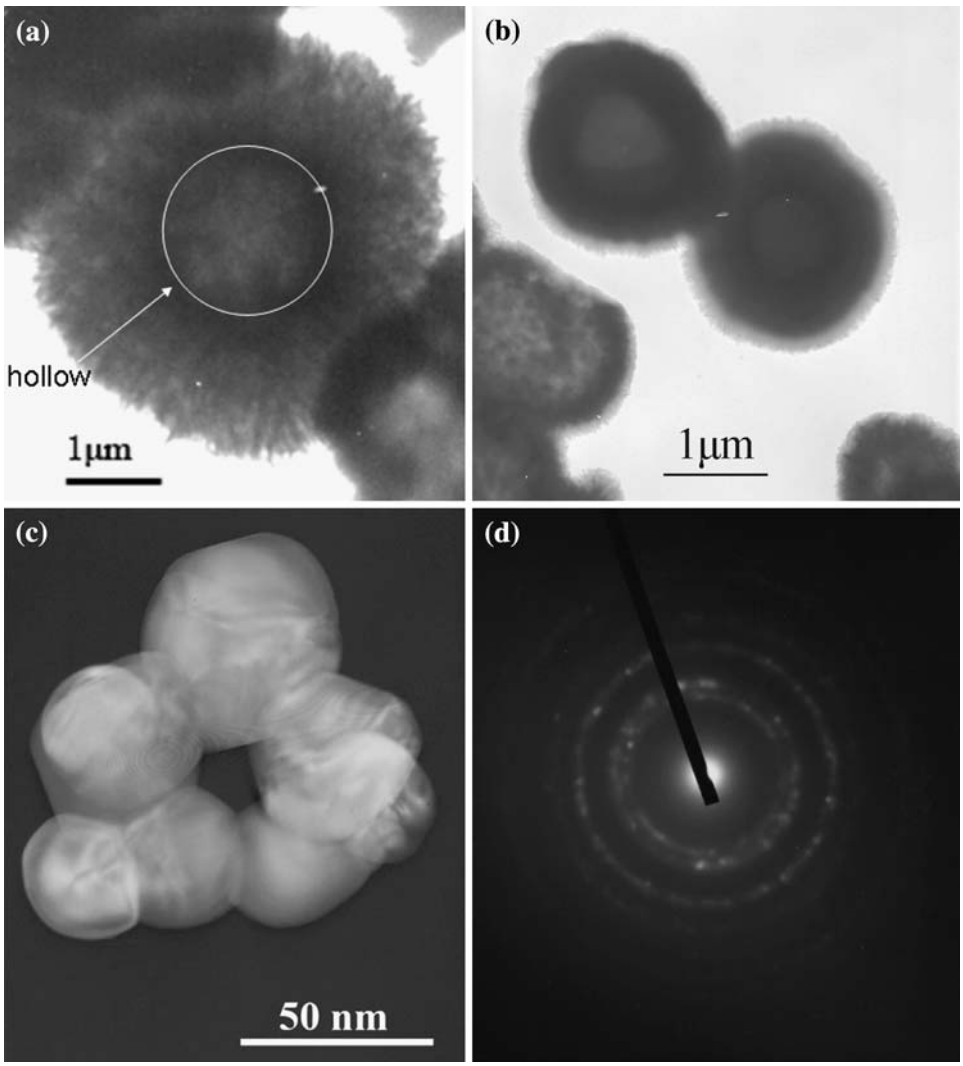

Fig. 3 TEM images of the samples. A hollow precursor sphere (the *white circle* shows the hollow structure) (**a**), the sample annealed at 300 °C (**b**), the fragments taken from the sample annealed at 500 °C (the structure of the hollow spheres was damaged during the ultrasonic agitation process) (**c**), and the selected area electron diffraction taken from the small particles shown in **c** (**d**)

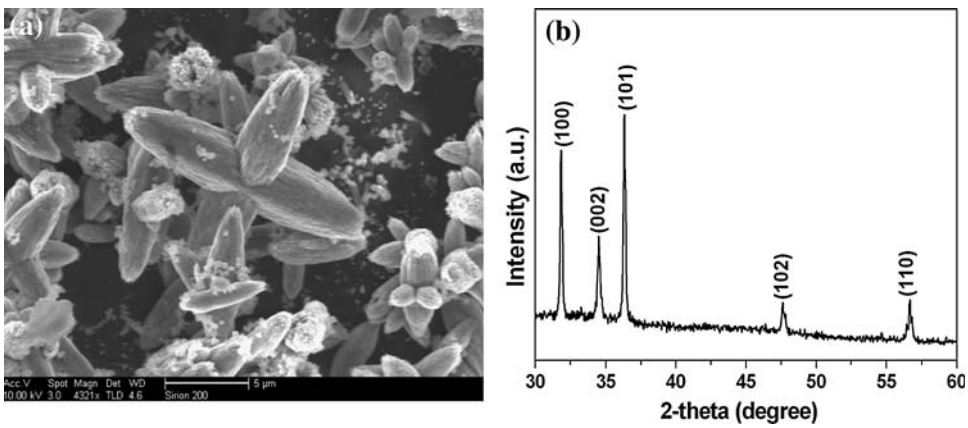

Fig. 4 FE-SEM (**a**) and XRD (**b**) of the sample prepared without the addition of citrate

The carbon element detected in EDS confirms the existence of carboxyl, which can be further proved by the FT-IR and TGA results. As shown in Fig. 5, the two strong peaks at 1,400 and 1,575 cm^{-1} that appeared in the precursor sample correspond to the vibration mode of carboxyl [25]. These peaks disappeared in the annealed sample. The peak at 470 cm^{-1} in the annealed sample is ascribed to ZnO vibration. The appearance of ZnO and disappearance of carboxyl vibration modes indicate the precursor had been completely converted into ZnO crystals at 500 °C. The TGA result is shown in Fig. 6. Below 300 °C, the curve shows a small weight loss, which is due

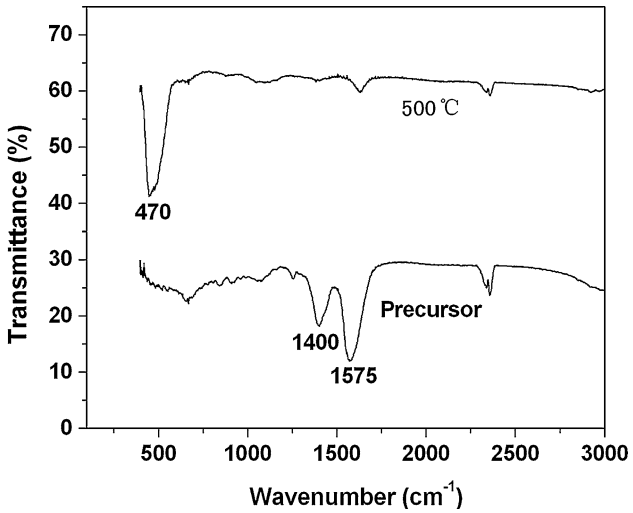

Fig. 5 FT-IR spectra of the precursor and annealed samples

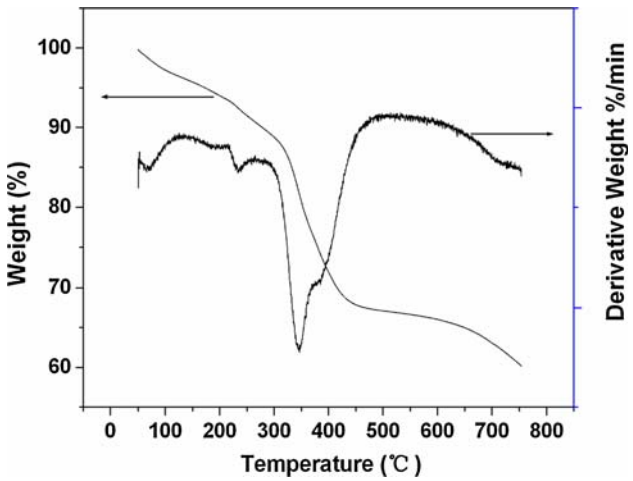

Fig. 6 TGA curves of the sample

to the removal of adsorbent water or gases. The large weight loss (about 25%) was observed at about 350 °C, indicating the breakdown of the organic composition in the citrate complex.

3.3 Nitrogen sorption

The porous structure of the resulting sample was studied by nitrogen sorption. Figure 7 presents the nitrogen adsorption-desorption isotherms and Barret–Joyner–Halenda (BJH) pore size distribution curves of the sample annealed at 300 °C. A hysteresis loop in the range of 0.4–1.0 P/P_0 in the isotherm curve was observed. The pore size of the ZnO hollow spheres was estimated to be 3.5 nm according to the pore size distribution curve (inset of Fig. 7). The pore size and BET surface area data measured from the samples annealed at different temperatures are shown in Table 1.

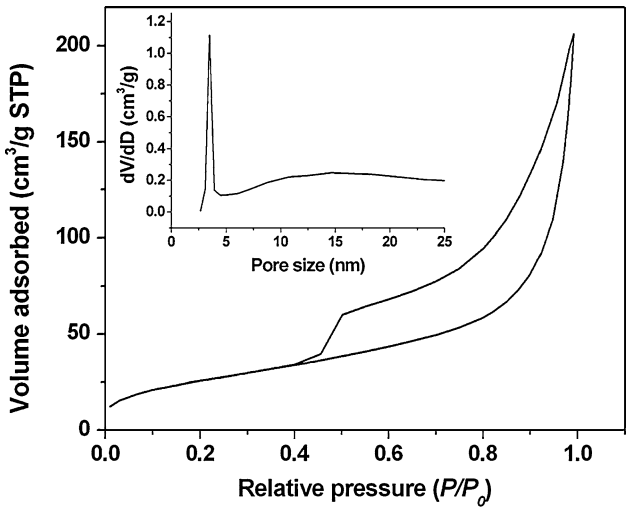

Fig. 7 Nitrogen adsorption-desorption isotherm and pore size distribution (inset) curves of the sample

Table 1 Pore size and BET surface area data measured from different samples

Samples	Pore size (nm)	BET surface area (m^2/g)
Precursor	9.8	45.3
Annealed at 300 °C	3.5	95.4
Annealed at 500 °C	20.6	18.2

Comparing it with the precursor sample, it can be seen that the pore size of the sample annealed at 300 °C decreased from 9.8 nm to 3.5 nm and the BET surface area increased from 45.3 m^2/g to 95.4 m^2/g. The reason for this change might be the decomposition of the organic substance, which left many small pores in the sample and increased the BET surface area. However, compared to the sample annealed at 500 °C, the pore size increased to 20.6 nm and the BET surface area decreased to 18.2 m^2/g, which resulted in the structural damage of the spheres and aggregation of ZnO nanocrystals.

3.4 Photocatalysis

The porous ZnO hollow spheres with high surface area are expected to be used in catalysis. To demonstrate the potential applicability of the products for the removal of contaminants from wastewater, we investigated the photocatalytic activity of different samples by employing the photocatalytic degradation of methyl blue test. In a typical process, 10 mg of ZnO hollow spheres (annealed at 300 °C) were added to 100 mL of 10^{-5} M methyl blue solution and magnetically stirred in the dark for 10 min. The solution was exposed to UV irradiation under a 300 W light source. The absorption spectra shown in Fig. 8a were recorded from the samples collected at different intervals.

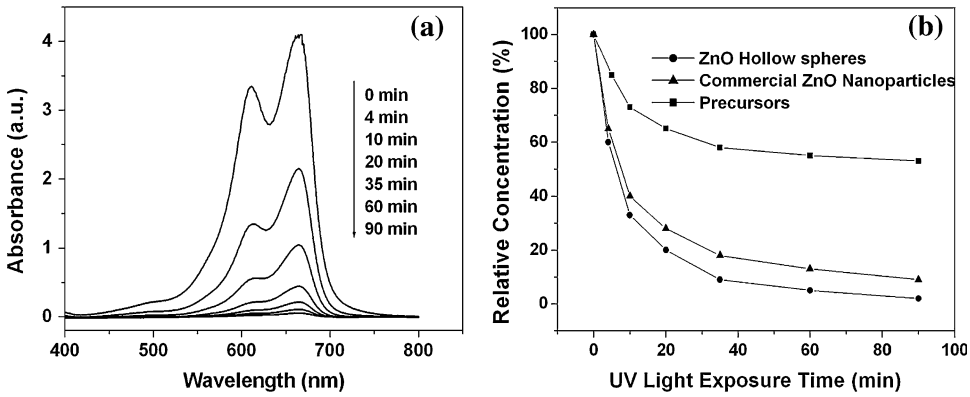

Fig. 8 Absorption spectra of methyl blue solution in the presence of ZnO hollow spheres under different exposure time (**a**) and the evolution of methyl blue concentration upon exposure time with different catalyst (**b**)

The concentration of methyl blue decreased rapidly with the increase of exposure time, indicating the photocatalytic degradation of the organic dyes. The commercial ZnO nanoparticles (100 nm in average diameter) and precursor materials were used as references to evaluate the photocatalytic performance of the ZnO hollow spheres. Figure 8b shows the changes in methyl blue concentration over the UV exposure time with different catalyst materials. It clearly shows the porous ZnO hollow spheres exhibit the highest photocatalytic performance. The high BET surface area and the improvement of crystalline quality are the possible reasons for the enhancement of photocatalytic activity.

4 Conclusions

ZnO hollow spheres have been successfully fabricated by calcination of hollow spherical precursor materials. The precursor was synthesized via a facile template-free aqueous solution method at low temperature. The products are porous in structure and have a large surface area. They exhibit superior photocatalytic activity during the photocatalytic degradation of methyl blue test, and may be useful in many applications, especially, when used as a photocatalyst.

Acknowledgment This work was financial supported by the Education Department of Guangxi Province (200708MS130) and Guilin University of Technology.

References

1. F. Caruso, R.A. Caruso, H. Mohwald, Science **282**, 1111 (1998). doi:10.1126/science.282.5391.1111
2. Q. Peng, Y. Dong, Y. Li, Angew. Int. Ed. **42**, 3027 (2003)
3. J. Bertling, J. Blomer, R. Kummel, Chem. Eng. Technol. **27**, 8290 (2004). doi:10.1002/ceat.200406138
4. D. Zhang, L. Qi, J. Ma, H. Cheng, Adv. Mater. **14**, 1499 (2002). doi:10.1002/1521-4095(20021016)14:20<1499::AID-ADMA1499>3.0.CO;2-5
5. D.Y. Wang, F. Caruso, Chem. Mater. **14**, 1909 (2002). doi:10.1021/cm0211251
6. S.L. Xiong, J.M. Shen, Q. Xie, Q. Gao, Q. Tang, Y.T. Qian, Adv. Funct. Mater. **15**, 1787 (2005). doi:10.1002/adfm.200500069
7. Y.Z. Li, T. Kunitake, S. Fujikawa, J. Phys. Chem. B **110**, 13000 (2006). doi:10.1021/jp061979z
8. X. Xu, S.A. Asher, J. Am. Chem. Soc. **126**, 7940 (2004). doi:10.1021/ja049453k
9. G. Zhu, S. Qiu, O. Terasaki, Y. Wei, J. Am. Chem. Soc. **123**, 7723 (2001). doi:10.1021/ja0158758
10. C.E. Fowler, D.D. Khushalani, S. Mann, Chem. Commun. (Camb.) **19**, 2028 (2001). doi:10.1039/b104879c
11. Z.X. Wang, M. Chen, L.M. Wu, Chem. Mater. **20**, 3251 (2008). doi:10.1021/cm8001223
12. L. Li, Y. Chu, Y. Liu, L. Dong, J. Phys. Chem. C **111**, 2123 (2007). doi:10.1021/jp066664y
13. Z.L. Wang, J. Phys. Condens. Matter. **16**, 829 (2004). doi:10.1088/0953-8984/16/25/R01
14. Z.W. Pan, Z.R. Dai, Z.L. Wang, Science **291**, 1947 (2001). doi:10.1126/science.1058120
15. Z.R. Tian, J.A. Voigt, J. Liu, B. Mckenzie, M.J. Mcdermott, J. Am. Chem. Soc. **124**, 12954 (2002). doi:10.1021/ja0279545
16. F. Li, Y. Ding, P. Gao, X. Xin, Z.L. Wang, Angew. Chem. Int. Ed. **43**, 5238 (2004). doi:10.1002/anie.200460783
17. M. Wang, C.H. Ye, Y. Zhang, G.M. Hua, H.X. Wang, M.G. Kong, L.D. Zhang, J. Cryst. Growth **291**, 334 (2006). doi:10.1016/j.jcrysgro.2006.03.033
18. Z.Q. Li, Y. Xie, Y.J. Xiong, R. Zhang, New J. Chem. **27**, 1518 (2003). doi:10.1039/b304787c
19. Q. Peng, S. Xu, Z.B. Zhuang, X. Wang, Y.D. Li, Small **1**, 216 (2005). doi:10.1002/smll.200400043
20. J.X. Duan, X.T. Huang, E.K. Wang, H.H. Ai, Nanotechnology **17**, 1786 (2006). doi:10.1088/0957-4484/17/6/040
21. Y.D. Yin, R.M. Rioux, C.K. Erdonmez, S. Hughes, G.A. Somorjai, A.P. Alivisatos, Science **304**, 711 (2004). doi:10.1126/science.1096566
22. A.D. Smigelskas, E.O. Kirkendall, Trans. AIME **171**, 130 (1947)
23. C.E. Birchenall, J. Electrochem. Soc. **103**, 619 (1956). doi:10.1149/1.2430174
24. Q. Wu, X. Chen, P. Zhang, Y. Han, X. Chen, Y. Yan, S. Li, Cryst. Growth Des. **8**, 3010 (2008). doi:10.1021/cg800126r
25. D. Mondelaers, G. Vanhoyland, H. Van den Rul, J. D'Haen, M.K. Van Bael, J. Mullens, L.C. Van Poucke, Mater. Res. Bull. **37**, 901 (2002). doi:10.1016/S0025-5408(02)00727-4